

Chapter 5

Sunyaev-Zeldovich effect due to “effervescent” heating and thermal conduction in galaxy clusters and groups

¹This chapter is based on the paper: Roychowdhury et al. , 2005, submitted to ApJ

Summary and the main results of chapter 5

Observations of the thermal Sunyaev-Zeldovich (SZ) effect in clusters and groups of galaxies probe the gas properties of the intracluster medium (ICM). Here we study the effect of a physically motivated non-gravitational “effervescent heating” mechanism on the thermal Sunyaev-Zeldovich effect in clusters. Our model of AGN heating also includes thermal conduction as another mechanism which also regulates the physical states of the intracluster gas. We also estimate the Poisson contribution to the angular power spectrum of the cosmic microwave background from the SZ effect due to AGN heating. This chapter discuss the results obtained:

- We show that the central decrement of the CMB temperature is reduced due to the enhanced entropy of the ICM, and that the decrement predicted from the plausible range of energy input from the AGN is consistent with available data of SZ decrement.***
- In addition, we also show that the “universal temperature” profile lowers the SZ decrement from that derived using the self-similar temperature profile.***
- We also find that the SZ signal is diminished as a result of AGN heating at all times in comparison to the default SZ signal, in contrast to the findings of Lapi et al. (2003).***
- We show that AGN heating, combined with the observational constraints on entropy, leads to suppression of higher multipole moments in the power spectrum and we find that this effect is stronger than previously thought. The suppression in the power spectrum in our model is due to depletion of gas from the central regions that is more efficient in low mass clusters and groups than in massive clusters.***

5.1 Introduction

The formation of structures in the Universe is believed to be hierarchical, as primordial density fluctuations, amplified by gravity, collapse and merge to form progressively larger systems. This hierarchical development leads to the prediction of self-similar scalings between systems of different masses and at different epochs (Peebles, 1980). These structures contain two components – the gravitationally dominant dark matter and the baryons contained in these potential wells whose response to processes other than gravitational interactions bring about deviations from the self-similar scalings.

Clusters and groups of galaxies contain dark matter and hot, diffuse gas called the intracluster medium. It was believed that this intracluster gas follows a self-similar scaling. However, recent observations of clusters and groups of galaxies have shown that the scalings are not self-similar. The observed relations of different physical parameters of the ICM such as density, temperature, X-ray luminosity and entropy have mostly confirmed the requirement for non-gravitational processes like AGN heating and radiative cooling (Lloyd-Davies et al 2000, Ponman et al. 2003, Sanderson et al. 2003, Pratt & Arnaud 2003, Pratt & Arnaud 2005). Simulations and theoretical models of clusters with gravitational processes alone also point to the fact that the entropy or X-ray luminosity observations can be matched only with non-gravitational heating (see chapter (2)). Many theoretical models have been proposed to explain these X-ray observations by heating from supernovae (Valageas & Silk 1999; Wu, Fabian & Nulsen 2000), radiative cooling (Bryan 2000; Voit & Bryan 2001; Muanwong et al. 2002; Wu & Xue 2002a; Davé, Katz & Weinberg 2002, Tornatore et al. 2003), accretion shocks (Tozzi & Norman 2001; Babul et al. 2002), quasar outflows (chapter (3)), and “effervescent heating” (chapter (4)). More information on various heating models can be found in a review by Gardini & Ricker (2004).

Until recently it was only X-ray observations that yielded information about the entropy excess. Due to advances in detectors and new observing strategies (Birkinshaw 1999, Grego et al. 2001; Grainge et al. 2002; Reese et al. 2002; Zhang & Wu 2000), the thermal Sunyaev-Zeldovich (SZ) effect (Sunyaev & Zeldovich 1972, 1980) is emerging as an *independent* test of the density and the thermal structure of clusters, thus equivalently of the entropy excess.

Many authors have investigated the role of excess entropy in clusters on the SZ effect and tried to quantify it (White et al. 2002; Springel et al. 2001; da Silva et al. 2001, 2004; Cavaliere & Menci 2001; Holder & Carlstrom 2001 & McCarthy et al. 2003a, 2003b). Holder & Carlstrom (2001), Cavaliere & Menci (2001) and McCarthy et al. (2003a) have also examined a few SZ scaling relations for individual clusters. They have shown that the SZ decrement is reduced in individual clusters as a result of energy injection and that the SZ scaling relations deviate from the self-similar predictions. In a more recent effort, Lapi et al. 2003 have estimated the enhancements in the SZ effect due to transient blastwaves from quasars and the depressions when the hydrostatic equilibrium is recovered.

In this chapter, we explore the consequences on SZ temperature decrement as a result of heating the intracluster medium via the “effervescent heating” mechanism (Begelman 2001, Ruszkowski & Begelman 2002, chapter (4)) and thermal conduction. We also focus on the SZ decrement resulting from the “universal temperature” profile” (see chapter (2)) and show that the earlier self-similar predictions due to pure gravity probably need to be revised. We also calculate the angular power

spectrum of the CMB due to effervescent heating and thermal conduction.

This chapter is organized as follows. In Section 2 we briefly describe our model. In Section 3 we estimate the central SZ decrements. We also simulate the evolution of the central SZ signal due to AGN heating, cooling and conduction. In Section 4 we estimate the angular power spectrum of the SZ temperature decrement in our models. We present our results and discussion in Section 5. Finally, our conclusions are summarized in Section 6.

In this chapter, we assume throughout that $\Omega_\Lambda = 0.71$, $\Omega_0 = 0.29$, $\Omega_b = 0.047$ and $h = 0.71$ which are the best fit parameters from WMAP (Spergel et al. 2003).

5.2 Model of the intracluster medium

5.2.1 The default state of the ICM

The details of the initial conditions of our model are similar to those adopted by (chapter (4)). In brief, we assume that the ICM is characterized by a “universal temperature profile” (Loken et al. 2002).

Density profiles are computed assuming hydrostatic equilibrium of the gas in the background dark matter potential. The background dark matter density profile is given by the self-similar Navarro, Frenk & White (NFW) profile (Komatsu & Seljak 2001) with a softened core (Zakamska & Narayan, 2003)

$$\rho_{\text{dm}} = \frac{\rho_s}{(r + r_c)(r + r_s)^2}, \quad (5.1)$$

where r_s is the standard characteristic radius of the NFW profile, r_c is a core radius inside which the density profile is a constant and ρ_s is the standard characteristic density of the usual NFW profile. The mass profile is given by

$$M_{\text{dm}}(\leq r) = 4\pi\rho_s r_s^3 m(x), \quad (5.2)$$

where $m(x)$ is a non-dimensional mass profile

$$\begin{aligned} m(x) &= \frac{x_c^2}{(1 - x_c)^2} \ln(1 + x/x_c) \\ &+ \frac{(1 - 2x_c)}{(1 - x_c)^2} \ln(1 + x) - \frac{1}{1 - x_c} \frac{x}{1 + x}, \end{aligned} \quad (5.3)$$

where $x = r/r_s$ and $x_c = r/r_c$. If $r_c = 0$, the usual mass distribution is recovered as in Komatsu & Seljak (2001). We follow Zakamska & Narayan (2003) and assume $r_c = r_s/20$. This is a reasonable choice as cluster lensing studies suggest that the core radius can be \sim tens of kilo-parsecs (Tyson et al., 1998; Shapiro & Iliev, 2000). We investigate the effect of the smoothing of the dark matter profile on our results.

5.2.2 Heating, thermal conduction and evolution of the ICM

The effervescent heating mechanism is a gentle heating mechanism in which the cluster gas is heated by buoyant bubbles of relativistic plasma produced by central AGN (Begelman 2000, Ruszkowski & Begelman 2002). The details of this model are already discussed in chapter (4).

The only two free parameters in this mechanism are the time averaged AGN luminosity, $\langle L \rangle$ and the time for which the heating continues, t_{heat} or rather a single free parameter, i.e. the total energy, $E_{\text{agn}} = \langle L \rangle t_{\text{heat}}$.

The flux due to thermal conduction F_{cond} is given by

$$\mathbf{F}_{\text{cond}} = -f\kappa\nabla T, \quad (5.4)$$

where κ is the Spitzer conductivity (for details, refer to §§§ (4.2.3.2) in chapter (4)), f is the suppression factor and T is the gas temperature. In our calculations, we adopt $f = 0.1$ (refer to §§§ (4.2.3.2) in chapter (4) for detail discussion).

The intracluster medium is evolved for a Hubble time, t_{H} , with heating, radiative cooling and conduction through a sequence of quasi-hydrostatic equilibrium solutions (see chapter (4)). The heating source is kept active for a time, $t_{\text{heat}} \ll t_{\text{H}}$. Then the gas is evolved with radiative cooling and convection alone till t_{H} . The boundary conditions imposed to solve for the physical state of the gas at each time-step, Δt , are: (1) the pressure at the boundary of the cluster, r_{out} , is constant and equal to the initial pressure at r_{200} , i.e., $P(r_{\text{out}}) = P_0(r_{200})$, and (2) the gas mass within r_{out} at all times is the same as the mass contained within r_{200} for the default profile at the initial time, i.e., $M_{\text{g}}(r_{\text{out}}) = M_{\text{g}0}(r_{200}) = 0.13M_{\text{dm}}(r_{200})$.

5.3 Thermal Sunyaev-Zeldovich effect

The temperature decrement of CMB due to the SZ effect is directly proportional to the Compton parameter (y). For a spherically symmetric cluster, the Compton parameter is given by

$$y = 2 \frac{\sigma_{\text{T}}}{m_{\text{e}}c^2} \int_0^R p_{\text{e}}(r) dl \quad (5.5)$$

where σ_{T} is the Thomson cross-section, and $p_{\text{e}}(r) = n_{\text{e}}(r)k_{\text{b}}T_{\text{e}}(r)$ is the electron pressure of the ICM, where $n_{\text{e}}(r) = 0.875(\rho_{\text{gas}}/m_{\text{p}})$ is the electron number density, k_{b} is the Boltzmann constant, and $T_{\text{e}}(r)$ is the electron temperature. The integral is performed along the line-of-sight (l) through the cluster and the upper limit of the integral ($+R$) is the extent of the cluster along any particular line-of-sight.

The angular temperature profile projected on the sky due to SZ effect, $\Delta T(\theta)/T_{\text{CMB}}$ is given in terms of the Compton parameter in equation (5.5)

$$\frac{\Delta T(\theta)}{T_{\text{CMB}}} = g(x)y(\theta), \quad (5.6)$$

where $g(x) \equiv x \coth(x/2) - 4$, $x \equiv hv/k_{\text{B}}T_{\text{CMB}}$, $T_{\text{CMB}} = 2.728$ (Fixsen et al. 1996). In the Rayleigh-Jeans approximation, $g(x) \approx -2$. We only evaluate ‘‘central’’ SZ decrement from the pressure profiles of our models. In this case, the integral in equation (5.5) reduces to

$$y_0 = 2 \frac{\sigma_{\text{T}}}{m_{\text{e}}c^2} \int_0^R p_{\text{e}}(r) dr \quad (5.7)$$

In the Rayleigh-Jeans part of the CMB spectrum, the deviation from the black-body spectrum results in a decrement of the CMB temperature,

$$\Delta T_{\mu w0} \approx -5.5 \text{ y K} \quad (5.8)$$

We use the pressure profiles resulting from our model to calculate the central SZ decrement in the temperature of the CMB.

5.4 Angular power spectrum

The angular two-point correlation function of the SZ temperature distribution in the sky is conventionally expanded into the Legendre polynomials:

$$\left\langle \frac{\Delta T}{T_{\text{CMB}}}(\hat{\mathbf{n}}) \frac{\Delta T}{T_{\text{CMB}}}(\hat{\mathbf{n}} + \theta) \right\rangle = \frac{1}{4\pi} \sum_l (2l+1) C_l P_l(\cos \theta) \quad (5.9)$$

Since we consider discrete sources, we can write $C_\ell = C_\ell^{(P)} + C_\ell^{(C)}$, where $C_\ell^{(P)}$ is the contribution from the Poisson noise and $C_\ell^{(C)}$ is the correlation among clusters (Peebles 1980, § 41). We define the frequency independent part in the power spectrum as $C_\ell^{*(P)} \equiv C_\ell/g^2(x)$. The integral expression of $C_\ell^{*(P)}$ can be derived following Cole & Kaiser (1988) as

$$C_\ell^{*(P)} = \int_0^{z_{\text{dec}}} dz \frac{dV}{dz} \int_{M_{\text{min}}}^{M_{\text{max}}} dM \frac{dn(M, z)}{dM} |y_\ell(M, z)|^2, \quad (5.10)$$

where $V(z)$ is the co-moving volume and y_ℓ is the angular Fourier transform of $y(\theta)$ given by

$$y_\ell = 2\pi \int y(\theta) J_0[(\ell + 1/2)\theta] \theta d\theta, \quad (5.11)$$

where J_0 is the Bessel function of the first kind of the integral order 0. In equation (5.10), z_{dec} is the redshift of photon decoupling and dn/dM is the mass function of clusters which is computed in the Press-Schechter formalism (Press & Schechter 1974). The mass function has been computed using the power spectrum for a λ -CDM model with normalization of $\sigma_8 = 0.9$. We choose $M_{\text{min}} = 5 \times 10^{13} M_\odot$ and $M_{\text{max}} = 2 \times 10^{15} M_\odot$ and integrate till redshift of $z = 5$ instead of z_{dec} . This is done because the integral in equation (5.10) is found to be insensitive to the upper limit in redshift beyond $z = 4$, the reason being that the mass function is exponentially suppressed beyond that redshift in this mass range.

5.5 Results

In this section, we discuss our results for the central SZ decrement for clusters with masses ranging from $M_{\text{cl}} = 5 \times 10^{13} - 2 \times 10^{15} M_\odot$. We first show the effects of the default temperature and density profiles of the ICM on the central SZ effect. Next we show the effects of heating and thermal conduction on the central SZ decrement.

In Figure (5.1), the central SZ temperature decrement $\Delta T_{\mu w0}$ is plotted as a function of the emission-weighted temperature of the cluster $\langle T \rangle$. The data points are a compilation of data sets from Zhang & Wu (2000) and McCarthy et al. (2003). The solid line shows the predicted $\Delta T_{\mu w0}$ from the default temperature profile and NFW potential. The dot-dashed line shows the predicted $\Delta T_{\mu w0}$ for

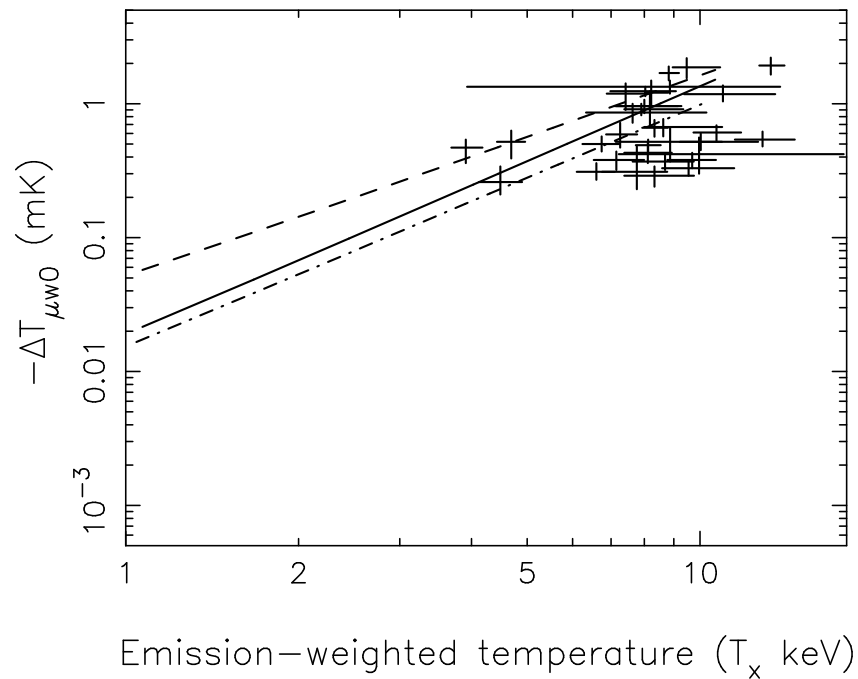


Figure 5.1: Observed and predicted $\Delta T_{\mu w 0} - \langle T \rangle$ relation of clusters. The solid line represents the predicted $\Delta T_{\mu w 0}$ with “universal” temperature profile (Loken et al. 2002), dark matter density profile given by NFW with $r_c = 0$ and the resulting density profile (chapter (2)). The dash-dotted line is the result of the dark matter profile given by NFW with $r_c = r_s/20$ and the ICM temperature profile as before. The dashed line is the result of self-similar profile (Wu & Xue 2002b, discussed in chapter (2)). The data points are from Zhang & Wu (2000) and McCarthy et al. (2003).

the same temperature profile but for smoothed NFW potential with $r_c = r_s/20$. The dashed line shows the prediction from the self-similar profile (Wu & Xue, 2002b (also discussed in chapter (2); Bryan 2000)).

It has been shown in chapter (2) that the density profile of gas is much flatter in comparison to the self-similar profile when it assumes the “universal temperature profile” and the standard NFW profile is assumed. As a result, the predicted central temperature decrement ($\Delta T_{\mu w0}$) is lower than that predicted by the self-similar model. The normalization of $\Delta T_{\mu w0}$ for a smoothed NFW profile with a core radius $r_c = r_s/20$ is even lower. This happens because the introduction of a core radius in the dark matter profile makes the ICM density profile shallower in the central regions as compared to the ICM density with a standard NFW profile. These decrements are closer to the data than predicted by earlier self-similar models for rich clusters.

Next we examine the effects of the “effervescent” heating, radiative cooling and conduction (model (B) discussed in chapter (4)) on the central SZ decrement. We evaluate $\Delta T_{\mu w0}$ for clusters in our sample after they have been evolved for a Hubble time t_H . The heating source was active for $t_{\text{heat}} \ll t_H$. The values of $\langle L \rangle$ and t_{heat} have been chosen so as to satisfy observational constraints on ICM entropy after t_H at $0.1 r_{200}$ and r_{500} (Ponman et al. 2003; see bottom panel of Figure (4.9) in the earlier chapter). In other words, there is a range of $\langle L \rangle$ that satisfies the entropy observations at a $1-\sigma$ uncertainty level that we used in our calculations. We used smoothed NFW profile with the core radius $r_c = r_s/20$.

In Figure 5.2, the shaded region is the expectation for the SZ central decrement when the gas is heated by the central AGN. The shaded region represents the spread in $\langle L \rangle$ which satisfies the entropy requirements at both radii, $0.1 r_{200}$ and r_{500} for $5 \times 10^8 < t_{\text{heat}} < 5 \times 10^9$ years. The solid line shows the prediction from self-similar profile (Wu & Xue, 2002b (discussed in chapter (2)); Bryan 2000).

In Figure 5.3, the evolution of the central SZ decrement $\Delta T_{\mu w0}$ is shown as a result of AGN heating, cooling and conduction (model (B) discussed in chapter (4)) for a cluster of mass $M_{\text{cl}} = 6 \times 10^{14} M_{\odot}$. The dashed line is the result of heating for $t_{\text{heat}} = 5 \times 10^8$ years and the solid line is the result of heating the ICM for $t_{\text{heat}} = 5 \times 10^9$ years. It can be seen that, as long as the heating source is active, $\Delta T_{\mu w0}$ decreases. When the source is switched off, $\Delta T_{\mu w0}$ starts to increase as the gas evolves only due to radiative cooling and conduction. This happens because the density, or equivalently the electron pressure, decreases when the gas is heated but becomes larger when it is allowed to cool. In addition, we have also plotted the default $\Delta T_{\mu w0}$ for the same cluster with a point denoted with an open circle. The central SZ decrement corresponding to our heating model is always lower than the default value.

Finally, we evaluate the Poisson contribution to the angular power spectrum of the SZ and compare our model predictions with earlier ones from self-similar models. In Figure (5.4), the thin solid line represents the angular power spectrum (Poisson) for the universal temperature profile and the corresponding density profile (chapter (3)). The dashed line is for self-similar model (Komatsu & Kitayama, 1999). The shaded region represents the angular power spectra calculated for the region of E_{agn} shown in the bottom panel of Figure (4.9) which satisfies the observed entropy at both radii for due to heating for $5 \times 10^8 < t_{\text{heat}} < 5 \times 10^9$ years.

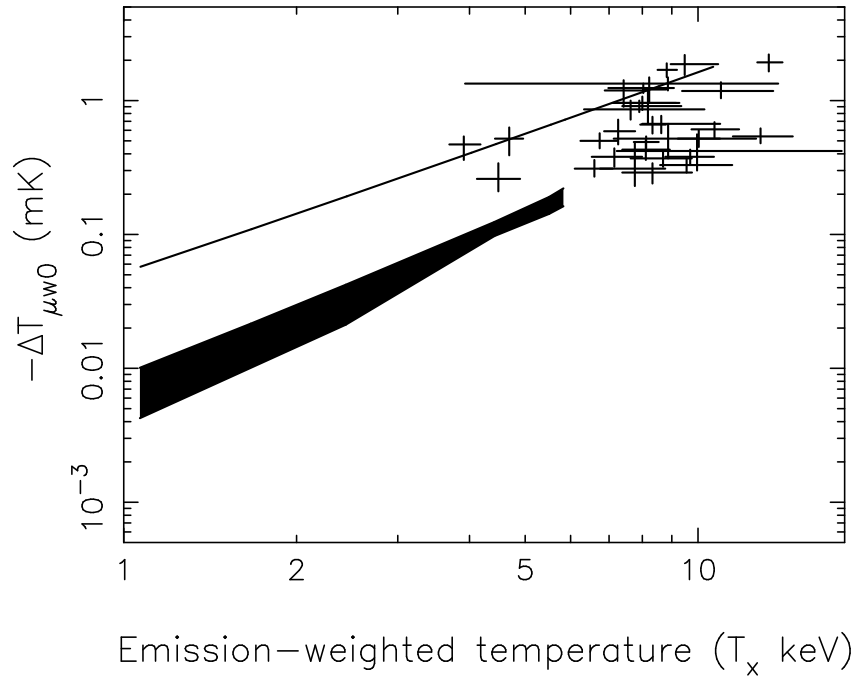


Figure 5.2: Observed and predicted $\Delta T_{\mu w 0} - \langle T \rangle$ relation of clusters evolved “effervescent” heating, thermal conduction and cooling ie. model (B) discussed in chapter (4). The solid line shows $\Delta T_{\mu w 0}$ for self-similar profile (Wu & Xue 2002b, also discussed in chapter (2)). The shaded region represents the SZ temperature decrement, $\Delta T_{\mu w 0}$, calculated for the region of E_{agn} shown in the bottom panel of Figure (4.9) which satisfies the observed entropy requirements at both radii for $5 \times 10^8 < t_{\text{heat}} < 5 \times 10^9$ years. The data points are from Zhang & Wu, 2000 and McCarthy et al. 2003.

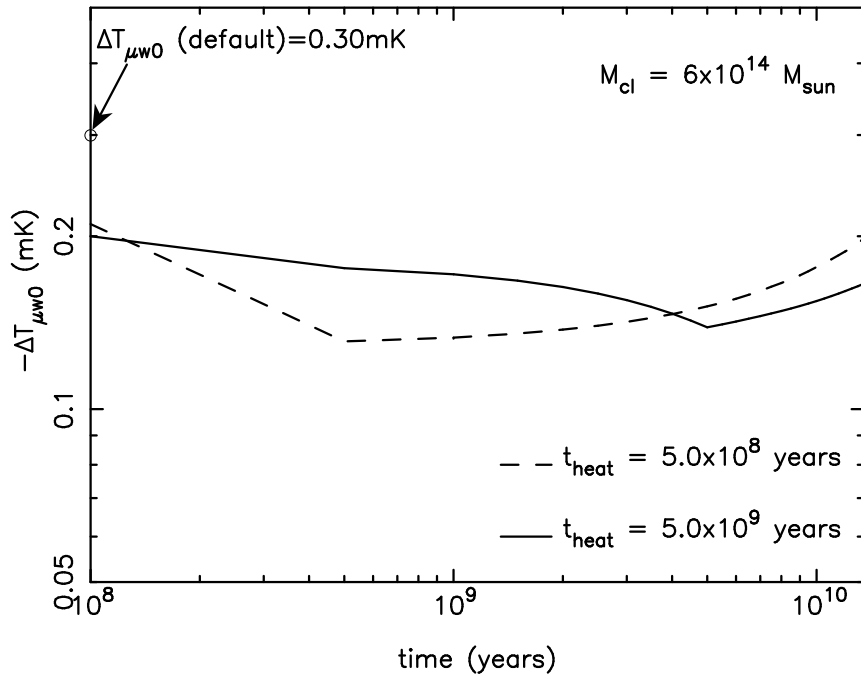


Figure 5.3: The evolution of the central SZ temperature decrement, $\Delta T_{\mu w 0}$, is shown for two different L_{agn} corresponding to the two values of t_{heat} for $M_{\text{cl}} = 6 \times 10^{14} M_{\odot}$ for model (B) ie. with AGN heating, conduction and cooling. The point denoted by an open circle is the value of $\Delta T_{\mu w 0}$ for the default profile with smoothed NFW ie. with a core for the same mass cluster.

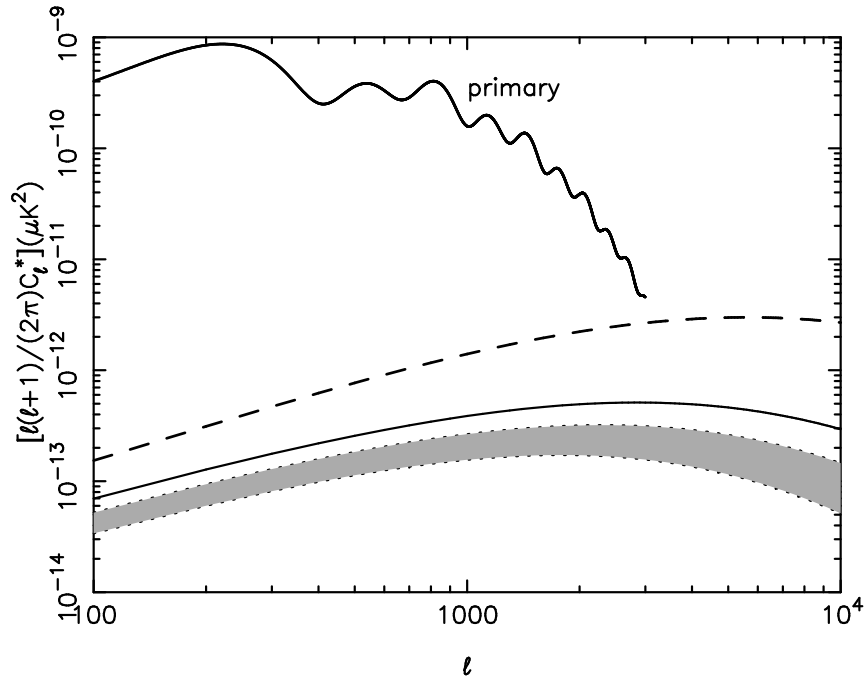


Figure 5.4: The Poisson contribution to the angular power spectrum (C_ℓ^*) of the SZ fluctuations is plotted here as a function of ℓ . The thick solid line is for the primary temperature anisotropy expected in the Rayleigh-Jeans band. The thin solid line is for the angular power spectrum (Poisson) due to the “universal temperature profile” of the cluster ICM and the dashed line is the expectation from a β - profile and isothermal temperature profile. The shaded region represents the angular power spectrum, C_ℓ^* , calculated for the region of E_{agn} shown in the bottom panel of Figure (4.9) which satisfies the observed entropy requirements at both radii for $5 \times 10^8 < t_{\text{heat}} < 5 \times 10^9$ years for model (B) discussed in chapter (4) where the cluster is heated by “effervescent” heating mechanism in the presence of thermal conduction and radiative cooling.

5.6 Discussion

In this chapter, we have examined the effects of effervescent heating by AGN with thermal conduction and radiative cooling in clusters (model (B) discussed in detail in chapter (2)) in the context of SZ temperature decrement.

As seen in Figure (5.1), the central SZ decrement for individual clusters is diminished if the “universal temperature profile” corresponding to the gravitational interactions of the ICM with the background dark matter is used. This reduces the discrepancy between the predicted central SZ signal and the observations compared to the predictions based on the standard self-similar profiles. The solid line in Figure (5.1) matches the observed points for rich clusters ($\langle T \rangle \leq 5$ keV) better than the dashed line, indicating that the requirement of non-gravitational heating for rich clusters is lower than previously thought. It is important to note here that the introduction of a core radius in the dark matter profile brings the SZ temperature decrements down further to match the observed points. This happens because the pressure profile of the intracluster medium becomes shallower in the central regions than for the NFW dark matter profile without smoothing.

We also find that the inclusion of effervescent heating, cooling and conduction have a significant effect on the SZ signal. The gas in the central region is depleted as a result of effervescent heating and thus we see a diminution in the SZ signal as a result of AGN heating. Similar conclusion was reached by McCarthy et al (2003a, 2003b) and Cavaliere & Menci (2001). However, in our case, there is a spread in the SZ signal. The spread reflects the fact that there is a range of energies required to satisfy the observed entropy at $0.1r_{200}$ and r_{500} for a particular t_{heat} . Shaded region in Figure (5.2) is based on fits of the heating model to the observational entropy data and is derived from the spread in E_{agn} in the bottom panel of Figure (4.9) in the earlier chapter that satisfies the observed entropy requirements at both radii for $5 \times 10^8 < t_{\text{heat}} < 5 \times 10^9$ years. As seen in Figure 5.2 the data for SZ are still not good enough to constrain heating models at present. We hope that future SZ observations of low temperature clusters will constrain the models better in the regime where discrepancies between self-similar and heating models are more pronounced.

We have also studied the time evolution of the SZ temperature decrement due to AGN heating, cooling and convection. It is seen in Figure (5.3) that the SZ signal is diminished as a result of AGN heating at all times in comparison to the default SZ signal. This is in contrast to the transient phases with *enhancement* of SZ signals predicted by Lapi et al. (2003) owing to strong feedback mechanisms that they assumed. Also, in the case of effervescent heating, the SZ decrement is lower than the default case even after the gas has evolved for a time $t_H - t_{\text{heat}}$ after the heating has been switched off. We note here that the values of $\langle L \rangle$ and t_{heat} have been chosen so as to satisfy the entropy requirements after evolving for t_H . The capabilities of future experiments like SZA are such that a decrement in the CMB temperature of $10 \mu\text{K}$ could be detected (S. Majumdar, private communication). This would mean that the lowest mass systems that SZA could observe would have $T \sim 2$ keV.

Finally, we also examine the effect of the universal temperature profile and AGN heating on the Poisson part of the angular power spectrum. We note that the peak of the SZ power spectrum is somewhat sensitive to the amount of heating that is added to the cluster gas. The peak of C_ℓ is at a lower l for a larger t_{heat} and at a higher ℓ for a smaller t_{heat} . Also, the effect due to heating is larger for higher values of ℓ . In our case the suppression takes place because the gas depletion from the

central regions is more efficient in low mass groups than in rich clusters. Therefore, the SZ signal is suppressed more efficiently at smaller scales and, thus, larger ℓ . We note that the general trend for the Poisson contribution to the spectrum to be suppressed at higher ℓ has been noted by others (Holder & Carlstrom, 1999; Kitayama & Komatsu 1999; Springel, White & Hernquist, 2001; Holder & Carlstrom 2001, Zhang & Wu 2003). This effect leads to a mismatch between the observed and theoretical spectra (Dawson et al. 2001, Mason et al. 2003) when preheating required to account for the entropy floor is considered. In our physically motivated effervescent AGN heating model, that fits the X-ray observations of entropy of the ICM, the power spectrum at small scales is even lower than previously thought. This suggests that other sources, such as, e.g., “dead” radio galaxy cocoons at higher redshifts (Yamada, Sugiyama & Silk 1999), should significantly contribute to anisotropies in the cosmic microwave background at large ℓ . We emphasize that our model deals only with global, average effect of heating on clusters and neglects small scale fluctuations in the gas distribution that are associated with heating.

5.7 Conclusion

The primary aim of this work has been to study the implications of the “effervescent heating” mechanism and thermal conduction on the SZ effect in galaxy clusters. We also evaluate the effect of the “universal” temperature profile on the SZ signal in order to re-calibrate the SZ expectations due to pure gravitational interactions.

The “effervescent heating” mechanism heats the gas in the central regions of clusters and makes the gas density profile shallower. This reduces the electron pressure of the gas and as a result reduces the SZ temperature decrement. This is in accordance with the findings of other authors (Cavaliere & Menci (2001), McCarthy et al. (2002), Lapi et al. (2003)). Here we have also shown how the SZ decrement would evolve as heating, cooling and convection regulate the physical state of the ICM. Our heating model is consistent with the available entropy data at $0.1r_{200}$ and r_{500} . We give specific predictions of our model for the SZ decrement for low mass (low temperature) clusters. Future observations performed with, e.g., Sunyaev-Zeldovich Array (SZA) or Combined Array for Research in Millimeter-wave Astronomy (CARMA) will be able to test these predictions.

We also point out that the “universal temperature profile”, that takes into account pure gravitational interactions, leads to lower SZ decrement than that calculated assuming that the ICM has a self-similar profile and is in better agreement with data for high $\langle T \rangle$ clusters. This implies that the discrepancy between observations and models without heating is reduced.

Finally, we also estimate the angular power spectrum of the CMB due to the SZ effect from Poisson distributed clusters. We show that the average effect of heating is to reduce the SZ signal and thus the angular power spectrum. The finding that the power spectrum at large ℓ is suppressed is consistent with previous results (e.g., Komatsu & Kitayama 1999, Holder & Carlstrom 2001). However, our results indicate that the contribution to the power spectrum that results from AGN heating, that is consistent with entropy measurements, is lower than previously thought. This suggests that other sources, such as, e.g., dead radio galaxy cocoons at higher redshifts (Yamada, Sugiyama & Silk 1999), should significantly contribute to small scale anisotropies of the cosmic microwave background.

Bibliography

Afshordi N., & Cen R., 2002, ApJ, 564, 669

Babul A., Balogh M. L., Lewis G. F., Poole G. B., 2002, MNRAS, 330, 329

Birkinshaw M., 1999, Phys. Rep., 310, 97

Begelman, M.C. 2001, in Gas and Galaxy Evolution, APS Conf. Proc., vol. 240, ed. Hibbard, J. E., Rupen, M.P., van Gorkom, J.H., p. 363, (astro-ph/0207656)

Bryan G. L., 2000, ApJ, 544, L1

Cavaliere A., Menci N., 2001, MNRAS, 321, 488

Cole S., Kaiser N., 1988, MNRAS, 233, 637

da Silva A. C. et al. , 2001, ApJ, 561, L15

da Silva A. C. et al. , 2004, MNRAS, 348, 140

Davé R., Katz N., Weinberg D. H., 2002, ApJ, 579, 23

Dawson K.S., Holzappel W. L., Carlstrom J. E., Joy M., LaRoque S. J., & Reese E. D., 2001, ApJ, 553, 1

Ettori S., 2003, MNRAS, 314, 729

Finoguenov A., Reiprich T. H., Böhringer H., 2001, A&A, 368, 749

Gardini, A., & Ricker, 2004, Mod. Phys. Lett., A19, 2317

Grainge K. et al. , 2002, MNRAS, 329, 890

Grego L et al. , 2001, ApJ, 552, 2

Holder G. P., Carlstrom J. E., 1999, in ASP Conf. Ser. 181, Microwave Foregrounds, ed. A. de Oliveira-Costa & M. Tegmark (San Francisco; ASP), 199

Holder G. P., Carlstrom J. E., 2001, ApJ, 558, 515

Komatsu E., Seljak U., 2001, MNRAS, 327, 1353

Komatsu E., Kitayama T., 1999, ApJ, 526, 1

Lapi A., Cavaliere A., De Zotti G., 2003, ApJ, 597, 93

Lloyd-Davies E. J., Ponman T. J., Cannon D. B., 2000, MNRAS, 315, 689

Loken C., Norman M. L., Nelson E., Bryan G. L., Motl P., 2002, ApJ, 579, 571

McCarthy I. G., Holder G. P., Babul A., Balogh M. L., 2003, ApJ, 591, 515

McCarthy I. G., Babul A., Balogh M. L., Holder G. P., 2003, ApJ, 591, 526

Muanwong O., Thomas P. A., Kay S. T., Pearce F. R., 2002, MNRAS, 336, 527

Navarro J. F., Frenk C. S., White S. D. M., 1996, ApJ, 462, 563

Navarro J. F., Frenk C. S., White S. D. M., 1997, ApJ, 490, 493

Nath B. B., Roychowdhury S., 2002, MNRAS, 333, 145

Peebles P. J. E., 1980, The Large-Scale Structure of the Universe, Princeton University Press, New Jersey

Pratt G. W., & Arnaud M., 2003, A&A, 408, 1

Pratt G. W., & Arnaud M., 2005, A&A, 429, 1

Press W. H., & Schechter P., 1974, ApJ, 187

Ponman T. J., Sanderson A. J. R., Finoguenov A., 2003, MNRAS, 343, 331

Reese E. D. et al., 2002, ApJ, 581, 53

Roychowdhury S., Nath B. B., 2003, MNRAS, 346, 199

Roychowdhury S., Ruszkowski M., Nath B. B., Begelman M. C., 2004, ApJ, 615, 681

Roychowdhury S., Ruszkowski M., Nath B. B., 2005, submitted to ApJ

Ruszkowski M., Begelman, M. C., 2002, ApJ, 581, 223

Sanderson A. J. R., Ponman T. J., Finoguenov A., Lloyd-Davies E. J., Markevitch M., 2003, MNRAS, 340, 989

Shapiro P. R., Iliev I. T., 2000, ApJ, 542, 1

Spergel D. N. et al., 2003, ApJS, 148, 195

Springel V., White M., Hernquist L., 2001, ApJ, 549, 681

Sunyaev R., Zeldovich Y., 1972, Comments Astrophys. Space Phys., 2, 66

Sunyaev R., Zeldovich Y., 1980, MNRAS, 190, 413

Tornatore L., Borgani S., Springel V., Matteucci F., Menci, N., & Murante G., 2003, MNRAS, 342, 1025

Tozzi P., Norman C., 2001, ApJ, 546, 63

Tyson J. A., Kochanski G. P., Dell' Antonio, 1998, ApJ, 498, 107

Valageas P., Silk J., 1999, A&A, 350, 725

Voit G. M., Bryan G. L., 2001, Nature, 414, 425

White M., Hernquist L., Springel V., 2002, ApJ, 579, 16

Wu K. K. S., Fabian A., Nulsen P. E. J. 2000, MNRAS, 318, 889

Wu X., Xue Y., 2002a, ApJ, 572, L19

Wu X., Xue Y., 2002b, ApJ, 569, 112

Yamada, M., Sugiyama, N. & Silk, J., 1999, ApJ, 522, 66

Zakamska N. L., Narayan R., 2003, ApJ, 582, 162

Zeldovich, Y. B., Sunyaev R. A., 1969, AP&SS, 4, 301

Zhang T., Wu X., 2000, ApJ, 545, 141

Zhang Y., Wu X, 2003, ApJ, 583, 529

A summary of the thesis

In this thesis, we have worked out the consequences of different models of active galaxy heating in clusters. The motivation for this work comes from the fact that X-ray observations show that the intracluster medium is heated by non-gravitational processes. Active galaxies are known to be one of the most energetic sources and are found inside clusters. Here, we have quantified the excess energy which AGNs can deposit into the ICM through jets, over-pressured cocoons and buoyant bubbles.

Chapter (2) aims at quantifying the gravitational expectations of entropy in the intracluster medium using the “universal temperature profile”. This helps us assess the excess entropy requirement in clusters by comparing this with recent X-ray observations. We use this as a benchmark in the later chapters when we evaluate the energetics of AGNs and their contribution to the intracluster medium.

In chapter (3), we model jets and over-pressured cocoons in quasars and estimate the energy a single quasar can contribute to the surrounding medium. In addition, we also estimate the statistics of quasars or AGNs inside a cluster of some mass ie. we derive the mass function of quasars inside clusters. Using these facts, we finally estimate the total excess energy which can be contributed by a population of quasars inside a cluster as a function of the cluster mass or temperature.

In chapter (4), we model the heating due to buoyant bubbles from an active galactic nuclei of the ICM. We consider two models of AGN heating here: one where “effervescent heating” is combined with convection and radiative cooling and the other where “effervescent heating” is combined with thermal conduction and cooling. We show that AGNs in this phase, which provides only gentle and have hardly any strong outflows, can also provide mechanical energy into the surrounding medium. We show that this energy is enough to heat the medium and raise its entropy so much so that it can satisfy the observed entropy values.

In chapter (5), we explore the ramifications of such heating via “effervescent mechanism” and thermal conduction of the intracluster gas on another observable property of the ICM, the thermal Sunyaev-Zel’dovich effect. We find that our heating models have some predictions which can be verified with new upcoming telescopes which are going to look at SZ effect from clusters. Infact, we find that non-gravitational heating in clusters would have considerable effects on the SZ temperature decrements and thus this can serve as another important constraint on such heating models of clusters.

Appendix A

Spherical Collapse Model

In the section on self-similar hierarchical collapse of structures § (1.2), we have mentioned the spherical collapse model for the growth of non-linear structures and also used its results. The present appendix is devoted to a description of this model and its results.

A.1 Description of the model

In this model, the time evolution of an over-dense region which is spherically symmetric is studied. Let us suppose that the over-dense region we are interested in has an initial density distribution

$$\rho(r, t_i) = \rho_b(t_i) + \delta\rho(r, t_i) = \rho_b(t_i)[1 + \delta_i(r)] \quad (\text{A.1})$$

where $\delta_i(r) = \delta(r, t_i)$ is the initial density contrast which is some specified, *non-increasing* function of r . Since we are now interested in perturbations with $\lambda \ll d_H$ (the horizon distance), the size R of the over-dense region (which is the scale over which δ_i is significant) can be taken to be much smaller than the Hubble radius. In such a case, it is possible to study the dynamics of this region using Newtonian approximation. In this limit, the proper radial coordinate $r = a(t)|\mathbf{x}|$ where \mathbf{x} is the co-moving Friedmann co-ordinate is used. The dynamics of this over-dense region is determined by the gravitational potential

$$\begin{aligned} \phi_{\text{total}}(r, t) &= \phi_b(r, t) + \delta\phi(r, t) = -\frac{1}{2} \left(\frac{\ddot{a}}{a} \right) r^2 + \delta\phi(r, t) \\ &= \frac{2\pi}{3} G\rho_b r^2 + \delta\phi(r, t) \end{aligned} \quad (\text{A.2})$$

where ϕ_b is the equivalent Newtonian potential of the Friedmann metric and $\delta\phi$ is the potential generated due to the excess density $\delta\rho(r, t)$. The motion of a thin shell of particles located at a distance r is governed by the equation

$$\frac{d^2\mathbf{r}}{dt^2} = -\nabla\phi_{\text{total}} = -\frac{4\pi G\rho_b(t)}{3}\mathbf{r} - \nabla(\delta\phi) = -\frac{GM_b}{r^3}\mathbf{r} - \frac{G\delta M(r, t)}{r^3}\mathbf{r} \quad (\text{A.3})$$

In writing the second term, we have used the fact that, for a spherically symmetric density distribution, the gravitational force only depends on the mass δM contained inside the shell. Here M_b and $\delta M(r, t)$ stand for

$$M_b = \frac{4\pi}{3}\rho_b(t)r^3 = \frac{4\pi}{3}\rho_b(t)a^3(t)x^3 = \text{constant}; \quad (\text{A.4})$$

and

$$\delta M(r, t) = 4\pi \int_0^r \delta\rho(r', t)r'^2 dr' = 4\pi\rho_b(t) \int_0^r r'^2 \delta(r', t) dr' \quad (\text{A.5})$$

To simplify the analysis of the problem, we also assume that the spherical shell do not cross each other during the evolution. In such a case, the mass contained within a shell of radius r does not change with time: $\delta M(r, t) = \delta M(r, t_i) = \text{constant}$. Thus we can write

$$\frac{d^2r}{dt^2} = -\frac{GM}{r^2}, \quad (\text{A.6})$$

where

$$M = \rho_b \left(\frac{4\pi}{3} r_i^3 \right) (1 + \bar{\delta}_i), \quad \bar{\delta}_i = \left(\frac{3}{4\pi r_i^3} \right) \int_0^{r_i} \bar{\delta}_i(r) 4\pi r^2 dr \quad (\text{A.7})$$

Here r_i is the initial radius of the shell with mass M and $\bar{\delta}_i$ is the average value of δ within r_i at time t_i . The first integral of Equation (A.6) is

$$\frac{1}{2} \left(\frac{dr}{dt} \right)^2 - \frac{GM}{r} = E \quad (\text{A.8})$$

where E is a constant of integration. The sign of E determines whether a given mass shell will expand forever or eventually decouple from the expansion and collapse. If $E > 0$, it follows from Equation (A.8) that \dot{r}^2 will never become zero; the shell will expand for ever along with the background space-time. On the other hand, if $E < 0$, then as r increases, \dot{r} will eventually become zero and later negative, implying a contraction and collapse.

This condition for the collapse of an over-dense region can also be expressed in a better way. Let us consider terms in the Equation (A.8) at the initial instant $t = t_i$, time at which δ is quite small and the over-dense region was expanding with the background. This means that the peculiar velocities V_i are negligible at $t = t_i$. Then, $\dot{r}_i = (\dot{a}/a)r_i = H(t_i)r_i \equiv H_i r_i$ at time t_i , and the initial kinetic energy is

$$K_i \equiv \left(\frac{\dot{r}^2}{2} \right)_{t=t_i} = \frac{H_i^2 r_i^2}{2} \quad (\text{A.9})$$

The potential energy at $t = t_i$ is $U = -|U|$ where

$$\begin{aligned} |U| &= \left(\frac{GM}{r} \right)_{t=t_i} = G \frac{4\pi}{3} \rho_b(t_i) r_i^2 (1 + \bar{\delta}_i) = \frac{1}{2} H_i^2 r_i^2 \Omega_i (1 + \bar{\delta}_i) \\ &= K_i \Omega_i (1 + \bar{\delta}_i) \end{aligned} \quad (\text{A.10})$$

with $\Omega_i = (\rho_b(t_i)/\rho_c(t_i))$ denoting the *initial* value of the density parameter Ω of the smooth background universe. The total energy of the shell is, therefore,

$$E = K_i - K_i \Omega_i (1 + \bar{\delta}_i) = K_i \Omega_i [\Omega_i^{-1} - (1 + \bar{\delta}_i)] \quad (\text{A.11})$$

The condition $E < 0$ for the shell to collapse (eventually), becomes $(1 + \bar{\delta}_i) > \Omega_i$, or

$$\bar{\delta}_i > [\Omega_i^{-1} - 1]. \quad (\text{A.12})$$

In a closed or flat universe (with $\Omega_i^{-1} \leq 1$), this condition is satisfied by any over-dense region ($\bar{\delta} > 0$). Thus over-dense regions will always collapse although smaller over-densities will take longer times to turn-around and collapse. Thus for a shell with $E < 0$, the maximum radius r_m which it attains is given by

$$\frac{r_m}{r_i} = \frac{(1 + \bar{\delta}_i)}{\bar{\delta}_i - (\Omega_i^{-1} - 1)} \quad (\text{A.13})$$

since $\dot{r} = 0$ at the instant of maximum expansion (using Equation (A.10) and Equation (A.11)). The time evolution of the shell can be found by integrating the equations of motion (Equation (A.8)).

A.2 Predictions for Einstein-de Sitter universe

For an Einstein-de Sitter universe, Equation (A.8) can be solved analytically (using parametric solutions) to get the time evolution of the mean density contrast of each shell, the maximum radius at

turn-around, r_m , the turn-around time, t_m or equivalently, turn-around redshift, z_m , and the average density contrast at turn-around, δ_m . They are as follows:

$$\begin{aligned} r_m &= \frac{3x}{5\delta_0}, \quad (1 + z_m) = \frac{\delta_0}{1.062}, \\ \left(\frac{\bar{\rho}}{\rho_b}\right)_m &= 1 + \delta_m = \frac{9\pi^2}{16} \approx 5.6, \end{aligned} \quad (\text{A.14})$$

where, $x = r_i[a(t)/a(t_i)]$ and $\delta_0 = (a(t)/a(t_i))(3\bar{\delta}_i/5) = (3/5)\bar{\delta}_i(1 + z_i)$. This is the present value of the density contrast, as predicted by the linear theory, if the density contrast was $\bar{\delta}_i$ at the redshift z_i .

In absence of shell-crossing, gravity would make the shell collapse back in a time-symmetric motion, so that the shell will reach the origin at $t = 2t_m$. Since shells are assumed to be composed of collisionless cold dark matter particles, they will simply pass through the centre, describing an oscillatory motion with amplitude r_m and period $2t_m$.

However, long before this happens, the approximation that matter is distributed in spherical shells and that random velocities of the particles are small, will break down. The collisionless dark matter will reach virial equilibrium by a process known as ‘violent relaxation’ (Lynden-Bell 1967). This will relax the dark matter component to a configuration with radius, r_{vir} , velocity dispersion v and density ρ_{coll} . After virialization of the collapsed shell, the potential energy U and the kinetic energy will be related by $|U| = 2K$ so that the total energy $\epsilon = U + K = -K$. At $t = t_m$ all the energy was in the form of potential energy. For a spherically symmetric system with a constant density, the total energy $\epsilon \approx -3GM^2/5r_m$. The ‘virial velocity’ v and the ‘virial radius’ r_{vir} for the collapsing mass can be estimated by the equations:

$$K \equiv \frac{Mv^2}{2} = -\epsilon = 3\frac{GM^2}{5r_m}; \quad |U| = \frac{3GM^2}{5r_{\text{vir}}} = 2K = Mv^2. \quad (\text{A.15})$$

The results are:

$$v = \left(\frac{6GM}{5r_m}\right)^{1/2}; \quad r_{\text{vir}} = \frac{r_m}{2} \quad (\text{A.16})$$

The time taken for the fluctuation to reach virial equilibrium, t_{coll} , is essentially the time corresponding to $t = 2t_m$. Thus we can find the collapse redshift, z_{coll} ,

$$(1 + z_{\text{coll}}) = \frac{\delta_0}{1.686}. \quad (\text{A.17})$$

Next, since $r_{\text{vir}} \approx r_m/2$, the mean density of the collapsed object is $\rho_{\text{coll}} \approx 8\rho_m$ where ρ_m is the density of the object at turn-around. Further, $\rho_m \approx 5.6\rho_b(t_m)$ and $\rho_b(t_m) = (1 + z_m)^3(1 + z_{\text{coll}})^{-3}\rho_b(t_{\text{coll}})$. Using these relations, we get

$$\rho_{\text{coll}} \approx 170\rho_b(t_{\text{coll}}) \approx 170\rho_b(1 + z_{\text{coll}})^3 \quad (\text{A.18})$$

where ρ_0 is the present cosmological density. Thus we have finally derived the average density contrast of a bound object in terms of the collapse redshift. The linearly extrapolated density contrast, δ_L at which an object collapses is $\delta_L = 1.686$. From the above result, we can see that the density contrast, for all collapsed objects, is the same at any particular collapse redshift (result used in § (1.2.1)).

Appendix B

Pre-heating Model of Kaiser (1991)

In the hierarchical picture of the formation of clusters, there are baryons which fall into the dark matter potential of clusters and get virialized to form the intracluster medium. This scenario leads us to believe that this baryonic gas which is trapped and virialized with the background dark matter would behave like it which would lead to it following the same scaling relations as that followed by the collisionless dark matter. However different observations have shown us that this is an over simplification and it is really not the case. This observed fact has led several authors to suggest that there is some agency which is heating this baryonic gas before it fell into the cluster potential. Thus after getting trapped in the cluster potential, it still retains that extra energy which was given to it before it got trapped into the cluster which leads it to have different scaling relations than the background dark matter clump.

In this appendix, we describe the pre-heating model proposed by Kaiser (1991) to break the self-similar scalings in clusters. He had proposed it to reconcile with the strong negative evolution in the X-ray luminosity of clusters.

B.1 The model

Kaiser (1991) assumed that at some early epoch, some astrophysical source (e.g. supernova explosions during the epoch of galaxy formation) injected sufficient energy into the gas to expel it from any then-existing dark matter potential well. This happened when the scale of non-linear clumps was much smaller than present-day rich clusters. Next, it was assumed (for simplicity) that this gas was raised to a uniform temperature, T_i and it had a density $\bar{\rho}_i = (8\pi/3)\Omega_{\text{gas}}H_i^2$; or that conditions are at least close to uniform when averaged over the mass scale of a present-day rich cluster (a co-moving radius $\simeq 10 h^{-1}$ Mpc). After the heat input, the gas would essentially be unperturbed by the dark matter clustering (since, T_i exceeds the virial temperature of the dark clumps then existing). However, as time goes by, the gas temperature will cool adiabatically with $T \propto a^{-2}$ (a is the scale factor of the universe), the potential wells will deepen and the gas will become more inhomogeneous. As the potential wells evolve, the gas will settle into them adiabatically, and shock (if any) would be weak. Actually, this assumption of Kaiser (1991) of the gas being isentropic through this process of merging and falling into the dark clumps and virializing was seconded by numerical simulations (Evrard 1990a, 1990b). During this process, the gas will contract until the gas temperature is roughly equal to the virial temperature of the confining dark clump. Using this fact and the assumption of adiabatic infall, the final gas density (ρ_f) can be derived. The assumption of adiabaticity gives

$$\begin{aligned} S_f \quad (\text{the final entropy}) &= S_i \quad (\text{the initial entropy of the gas}) \\ \Rightarrow \quad \rho_f &\simeq \bar{\rho}_i \left(\frac{\Phi}{T_i} \right)^{3/2}, \end{aligned} \quad (\text{B.1})$$

where final temperature of the gas, $T_f \propto \Phi$, the gravitational potential of the dark matter clump and as, gas entropy, $S_{\text{gas}} \propto T_{\text{gas}}/\rho_{\text{gas}}^{2/3}$.

Next we need to find the final radius of this gas cloud. For estimating this, we need to know the mass of gas which has fallen in. The gas mass which has fallen in is estimated as follows: at large radii, the gas will be in free fall with a velocity, $v_{\text{infall}} \sim H_c^{-1} \nabla \Phi \sim H_c^{-1} \Phi/r$, where the subscript ‘c’ denotes the epoch at which we observe the cluster. Now, the maximum radius of the

region from which material can fall into the cluster potential within a Hubble time, $t_H \simeq 1/H_c$, would be fixed by the fact that it has to be a region within which the infall velocity, v_{infall} , would be enough to transport the material to the centre of the cluster within a Hubble time, $t_H \simeq 1/H_c$. Thus,

$$\begin{aligned} r_0 &\simeq v_{\text{infall}} \times t_H \simeq H_c^{-1} \frac{\Phi}{r_0} \times \frac{1}{H_c} \\ &\simeq \frac{\Phi^{1/2}}{H_c} \end{aligned} \quad (\text{B.2})$$

Thus all the material which is interior to this radius, r_0 , would fall together and virialize to form the intracluster medium. Assuming this, the final gas radius r_f can be estimated by mass conservation i.e. equating $\rho_f r_f^3$ and $\bar{\rho}_i r_0^3$ and using Equation (B.1) and Equation (B.2),

$$\begin{aligned} r_f^3 &\simeq \frac{\bar{\rho}_i r_0^3}{\rho_f} \\ \Rightarrow r_f &\simeq \frac{T_i^{3/2} \Omega_{\text{gas}}}{\bar{\rho}_i H_c} \end{aligned} \quad (\text{B.3})$$

Using the above result (B.3), we estimate the X-ray luminosity

$$\begin{aligned} L_x &\sim \rho_f^2 r_f^3 T_f^{1/2} \\ &\sim \frac{\bar{\rho}_i}{T_i^{3/2}} \Phi^{7/2} \Omega_{\text{gas}} H_c^{-1} \end{aligned} \quad (\text{B.4})$$

So, Equation (B.4) shows the scaling of L_x with gas temperature, T_f . As we see from Equation (B.4), $L_x \propto T_f$ and not $\propto T_f^2$.

So, in this model of Kaiser (1991), where the gas is pre-heated before it falls into the cluster, he showed that pre-heated gas have scaling relations which are different from self-similar scalings and that this scenario can explain the X-ray observations of intracluster medium.